NASA

Technical Memorandum 83810

Accreting White Dwarf Models for Type I Supernovae. I. Presupernova Evolution and Triggering Mechanisms

Ken'ichi Nomoto

AUGUST 1981

National Aeronautics and Space Administration

Goddard Space Flight Center
Greenbelt, Maryland 20771

ACCRETING WHITE DWARF MODELS FOR TYPE I SUPERNOVAE.

I. PRESUPERNOVA EVOLUTION AND TRIGGERING MECHANISMS

Ken'ichi Nomoto[1]

Laboratory for Astronomy and Solar Physics

NASA-Goddard Space Flight Center

Received: _____

[1] On leave from Department of Physics, Ibaraki University, Japan

ABSTRACT

As a plausible explosion model for a Type I supernova, the evolution of carbon-oxygen white dwarfs accreting helium in binary systems has been investigated from the onset of accretion up to the point at which a thermonuclear explosion occurs. Although the accreted material has been assumed to be helium, our results should also be applicable to the more general case of accretion of hydrogen-rich material, since hydrogen shell burning leads to the development of a helium zone.

Several cases with different accretion rates of helium and different initial masses of the white dwarf have been studied. The relationship between the conditions in the binary system and the triggering mechanism for the supernova explosion is discussed, especially for the cases with relatively slow accretion rate.

It is found that the growth of a helium zone on the carbon-oxygen core leads to a supernova explosion which is triggered either by the off-center helium detonation for slow and intermediate accretion rates or by the carbon deflagration for slow and rapid accretion rates. Both helium detonation and carbon deflagration are possible for the case of slow accretion, since in this case the initial mass of the white dwarf is an important parameter for determining the mode of ignition. Finally, various modes of building up the helium zone on the white dwarf, namely, direct transfer of helium from the companion star and the various types and strength of the hydrogen shell flashes are discussed in some detail.

Subject headings: stars: accretion - stars: binaries -
stars: evolution - stars: interiors - stars: supernovae
- stars: white dwarfs

I. INTRODUCTION

a) Type I Supernovae

The origin of Type I supernovae (SN I) has long been obscure (see Wheeler 1981 for a review). The spectra of SN I show no strong hydrogen lines, which implies that the progenitor stars of SN I should be hydrogen-deficient stars (e.g. Oke and Searle 1974). SN I have been observed in elliptical galaxies as well as in spiral and irregular galaxies (e.g. Tammann 1974). SN I are not concentrated in spiral arms (Maza and van den Bergh 1976). These facts have led to the ideas that the progenitor stars of SN I are white dwarfs (Finzi and Wolf 1967; Whelan and Iben 1973) or helium stars (Wheeler 1978; Arnett 1979).

Another characteristic of SN I is the exponential tail in their light curves (e.g. Barbon, Ciatti, and Rosino 1973). Such a tail requires an additional energy source at late times. Several energy sources have been proposed (see Chevalier 1981a for a review). Among them, the radioactive decay model ($^{56}Ni \rightarrow {}^{56}Co \rightarrow {}^{56}Fe$) has recently made remarkable advances (Arnett 1979; Colgate, Petscheck, and Kriese 1980; Axelrod 1980 a,b; Chevalier 1981b; Weaver, Axelrod, and Woosley 1980). It has been shown that energy deposition of γ-rays and positrons emitted from the decays of ^{56}Ni and ^{56}Co can produce a good fit to the observed light curves of SN I. This model is supported by the good agreement between the observed spectra of SN I 1972e at late times (Kirshner and Oke 1975) and the calculated synthetic spectra of Fe (Meyerott 1980) and of Fe with

Co (Axelrod 1980a,b).

The above success gives an important constraint on the progenitor models for SN I, i.e., relatively large amount of ^{56}Ni should be produced through the primary explosion. Therefore we need to investigate whether the candidate stars of SN I actually evolve to produce sufficient ^{56}Ni during the explosions. I have made such a computation for the evolution of accreting white dwarfs from the beginning of the mass accretion through the explosion.

b) Evolution of Accreting White Dwarfs

A white dwarf in a close binary system can evolve into a supernova explosion in the following way. When the companion star begins to expand over its Roche lobe, the white dwarf accretes the matter transferred from the companion star. When a sufficient amount of hydrogen-rich material is accumulated on the white dwarf, hydrogen shell burning is ignited. The hydrogen burning can proceed either in a thermally stable fashion or through unstable shell-flashes.

The strength of the shell-flashes depends mainly on the accretion rate (see Sugimoto and Miyaji 1980 for a review). Rapid accretion leads to a stable hydrogen burning or a relatively weak shell flash which process most of the accreted matter into helium. Slower accretion results in a stronger flash (sometimes nova-like explosion) which ejects a part of the accreted matter into space while processing the rest of the material into helium. Such hydrogen shell flashes recur many times

during the accretion, and a helium zone gradually grows in mass near the surface of the white dwarf; this is equivalent to the accretion of helium. It is also possible that helium is directly transferred from the companion star because, in some cases of mass exchange, the companion star might have evolved into a helium star before filling its Roche lobe. (See §V for a more detailed discussion on the relationship between the strength of the hydrogen shell flashes, the growth of the helium zone and the conditions in the binary system and for a discussion of the possible evolutionary scenario leading to the direct accretion of helium.)

The effect of the growing helium zone on the evolution of accreting helium white dwarfs was first investigated by Nomoto and Sugimoto (1977). They simulated the average evolution by computing the steady accretion of helium, which is a good approximation as far as the phenomena in the relatively deep layers interior to the hydrogen-burning shell are concerned. It was found that relatively rapid accretion ignites the weak off-center helium flash while slow accretion leads to the ignition of helium at the center. In the latter case, the white dwarf disrupts completely as a helium detonation supernova and ejects a large amount of ^{56}Ni (see also Mazurek 1973).

Recently the same approach was adopted by Fujimoto and Sugimoto (1979, 1981, hereafter referred to as FS) and Taam (1980a,b, hereafter referred to as TM) for the study of long term evolution of accreting carbon and oxygen (C+O) white dwarfs. They showed that, in some cases of accretion, the building up of a substantial helium zone on the C+O white dwarf leads to a very explosive helium shell flash that could

trigger a supernova-like explosion. However, their results were preliminary because they assumed hydrostatic equilibrium in their computations and stopped computing at the beginning of the hydrodynamical stages.

c) Present Study

I have investigated the evolution of C+O white dwarfs by adopting the same method as Nomoto and Sugimoto (1977) starting from the onset of accretion of helium through the thermonuclear explosions, i.e., from the hydrostatic through hydrodynamic stages. Several cases with different accretion rates of helium and different initial masses of the white dwarf have been computed. I have found that the accreting C+O white dwarfs actually evolve into supernovae of various types, namely, double detonation, single detonation, and carbon deflagration, depending on the conditions at the initiation of the explosion. Most of these models produce a large amount of ^{56}Ni as required by the radioactive decay model for the light curve of SN I.

In the present series of papers (I - III), these numerical results are described in detail and the various types of white dwarf models for SN I are presented. The preliminary results have been published in the proceedings of several workshop and symposia (Nomoto 1980a,b,c; see also Woosley, Weaver, and Taam 1980). In this Paper I, I discuss the presupernova evolution of the white dwarfs, namely, growth of a helium zone, ignition and progress of the strong flash, and the transition from hydrostatic through hydrodynamical stages. Cases with the relatively

slow accretion and high initial mass of the white dwarf are investigated especially in detail, for which the results by FS and TM were only preliminary. Then the refined relationship between the triggering mechanisms of SN I and the conditions in the binary system (i.e., the accretion rate and the initial mass of the white dwarf) is presented. In the subsequent papers (II, III), the hydrodynamic behavior of the supernova explosions, i.e., the formation and propagation of the detonation wave and deflagration wave will be discussed. These models will be compared with the observations of SN I.

In the next section, the assumptions and numerical methods are described. Evolution from the onset of accretion through the early hydrodynamical stages are discussed in §III and the dependence of the mode of ignition on the parameters are summarized in §IV. In §V, the various modes of building up the helium zone, i.e., a rapid accretion of helium and the various types of hydrogen shell burning in the accreting white dwarfs are discussed.

II. PHYSICAL INPUT

The method of computation and the physical input in the present investigation are mostly the same as those used by Nomoto and Sugimoto (1977) and thus are briefly summarized here. Hereafter, the normal notations (see Appendix in Sugimoto and Nomoto 1980) are used unless otherwise stated.

The evolution from the beginning of the accretion all the way through explosion was computed by using a Henyey-type hybrid (implicit-explicit) method to include both thermal and hydrodynamical equations (see Sugimoto 1970; Nomoto and Sugimoto 1977; Nariai, Nomoto, and Sugimoto 1980). Spherical symmetry was assumed.

For the shock propagation, the artificial viscosity (Richtmeyer and Morton 1967), Q, defined by

$$Q = \begin{cases} \ell^2 \rho r^2 \left(\frac{\partial (v/r)}{\partial r}\right)^2 & \text{if } \frac{\partial (v/r)}{\partial r} < 0, \\ 0 & \text{otherwise,} \end{cases} \qquad (1)$$

(e.g. Appenzeller 1970) was used, where $\underline{v}$ denotes the velocity and the parameter ℓ was assumed to be $2\Delta r$ (Δr denotes the distance between the adjacent zone boundaries). For convection, the time-dependent mixing length theory as formulated by Unno (1967) was applied (see Nomoto and Sugimoto 1977 for the expression). The radiative and conductive opacities were calculated by using Iben's (1975) analytic approximations except for

the Compton scattering opacity to include the effect of electron-degeneracy (Sampson 1961).

Composition of the C+O white dwarf was assumed to be $X_C = X_O = 0.5$ where X_C and X_O denote the abundances of carbon and oxygen, respectively. The equation of state for partially relativistic and partially degenerate electrons included electron-positron pairs (Sugimoto and Nomoto 1975b). The effects of Coulomb interactions were taken into account by applying Van Horn's (1969, 1971) approximation for the liquid state and Salpeter's (1961) formula for the solid state. The Debye function for specific heats was included. The effects of crystalization (Pollock and Hansen 1973) were taken into account.

For the nuclear reactions, the rates given by Fowler, Caughlan, and Zimmerman (1975), the weak and intermediate screening factors by Graboske et al. (1973) and the strong screening factors by Itoh et al. (1977, 1979) complemented by Alastuey and Jancovici (1978) were used. For the pycnonuclear regime of carbon burning, the reaction rate by Salpeter and Van Horn (1969) under the static lattice approximation was used. The nuclear statistical equilibrium composition including electron capture rates was calculated by applying the same data used by Yokoi, Neo, and Nomoto (1979).

It should be noted here that, for some white dwarfs with relatively slow accretion rates, the interior temperature is much lower than in normal stars (see §III) so that the applicability of the 3α reaction rate by Fowler et al. (1975) must be examined. For relatively high temperatures ($T > 8 \times 10^7$K), the 3α process is a resonant reaction. For lower temperatures, however, the 3α process can no longer be regarded as a

resonant reaction so that a nonresonant reaction rate should be used (Cameron 1959). Since Fowler et al. (1975) give only the resonant 3α reaction rate, I have calculated the nonresonant reaction rates for the α+α and ^{8}Be+α reactions according to the recipe of Clayton (1968) by using the nuclear data of Barnes (1980). The ratios thus obtained between the nonresonant (NR) and the resonant (R) reaction rates are given by

$$\hat{r}_{Be+\alpha} \equiv \frac{\langle\sigma v\rangle_{NR}}{\langle\sigma v\rangle_{R}}\Big|_{Be+\alpha} \tag{2}$$

$$= 2.64 \times 10^{4} T_8^{-1/2} \exp\,(33.3\, T_8^{-1} - 50.8\, T_8^{-1/3})(T_8^{-2/3} - 0.507)^{-2},$$

and

$$\hat{r}_{\alpha+\alpha} \equiv \frac{\langle\sigma v\rangle_{NR}}{\langle\sigma v\rangle_{R}}\Big|_{\alpha+\alpha} \tag{3}$$

$$= 7.20 \times 10^{2} T_8^{-1/2} \exp\,(10.7\, T_8^{-1} - 29.1\, T_8^{-1/3})(T_8^{-2/3} - 0.907)^{-2},$$

for ^{8}Be+α and α+α reactions, respectively, where $T_8 \equiv T/10^8$K. Since the NR reaction rate has a much weaker temperature dependence than the R rate, these ratios exceed unity for very low temperatures; in fact, $\hat{r}_{Be+\alpha} > 1$ for $T_8 \lesssim 0.74$ and $\hat{r}_{\alpha+\alpha} > 1$ for $T_8 \lesssim 0.28$. Therefore, the 3α reaction rate by Fowler et al. (1975) has been multiplied by $\hat{r}_{Be+\alpha}$ for $0.28 \lesssim T_8 \lesssim 0.74$ and by $\hat{r}_{Be+\alpha}\cdot\hat{r}_{\alpha+\alpha}$ for $T_8 \lesssim 0.28$. Since these NR reaction rates were not included by either FS or TM, they did not find the ignition of helium at temperatures as low as $T_8 < 0.5$. However, the NR reaction rate is greatly enhanced by strong screening at high density even for $T_8 < 0.5$

so that the evolution of a low temperature white dwarf should be greatly different from that found in the previous studies (see §III).

III. RESULTS

a) Initial Models and Parameters

The parameters for the initial models of the C+O white dwarfs are summarized in Table 1. Hereafter the superscript (0) denotes the initial value just before the onset of accretion, and the initial mass is denoted by $M_{C+O} \equiv M^{(0)}$. The 1.08 $M_\odot$ white dwarf model was constructed from the 1.08 $M_\odot$ C+O core in the 7 $M_\odot$ red giant star of Sugimoto and Nomoto (1975a). The core was allowed to cool down for 10^8yr after the stripping off of the hydrogen-rich envelope. The initial models with larger masses were constructed from the 1.08 $M_\odot$ model by increasing the mass artificially and again permitting them to cool. These white dwarfs have helium envelopes as thin as $10^{-5}M_\odot$.

The evolution of a white dwarf during the accretion phase was simulated by adopting the same method as Nomoto and Sugimoto (1977), i.e., by assuming that the helium zone grows in mass at a constant accretion rate of dM/dt. The effect of the hydrogen shell flashes was neglected; the nuclear energy released by the flashes is mostly radiated away during the relatively long interflash accretion phases and the gravitational energy release by the accreted helium has much larger effects on the deep helium layers (Nomoto and Sugimoto 1977). I computed six cases A-F for different accretion rates of helium, dM/dt, and the initial masses, M_{C+O}, as summarized in Table 1.

b) Evolution During the Accretion Phase

i) Thermal Effects of Accretion

The accreted matter gradually forms a helium zone on the C+O core and thus increase the white dwarf mass, M. As a result, the matter in the interior is compressed to higher densities as seen in Figure 1[2], where the changes in the density distribution for cases A and C are shown. Such compression of the interior by accretion releases gravitational energy and increases the interior temperature. At the same time, the accreting white dwarf loses energy by emitting photons and neutrinos at a rate of L_{ph} and L_ν, respectively.

These competitive effects on the interior temperature are shown by the energy conservation equation as

$$\int_0^M \left(\frac{\partial u}{\partial \ln T}\right)_\rho \frac{d\ln T}{dt}\, dM_r = \int_0^M \left[\frac{P}{\rho} - \left(\frac{\partial u}{\partial \ln \rho}\right)_T\right] \frac{d\ln \rho}{dt}\, dM_r - L_{ph} - L_\nu \qquad (4)$$

where $\underline{u}$ denotes the specific internal energy. In the strongly electron-degenerate state (i.e., $\psi >> 1$ where ψ denotes the chemical potential of the electron in units of kT and $\underline{k}$ denotes the Boltzman constant), the coeficient of the Pd $(1/\rho)$ work term in equation (4) is as small as

$$1 - \left(\frac{\partial u}{\partial \ln \rho}\right)_T \frac{\rho}{P} \simeq \frac{k}{\mu_I H} \frac{\rho T}{P} \simeq \frac{\mu_e}{\mu_I} \frac{5}{2\psi} << 1 \qquad (5)$$

---

[2] In Figures 1-9, the white dwarf mass is denoted by M_{WD}.

where the Coulomb interactions between electrons and ions are neglected for simplicity and μ_e, μ_I, and H denote the mean molecular weight per electron and per ion, and atomic mass unit, respectively (see Van Horn 1971). This implies that most of the gravitational energy release goes into increasing the Fermi energy of the electrons and only a fraction contributes to increasing the internal temperature (Van Horn 1971). Therefore the effect of the gravitational energy release is negligible for the cooling of a constant mass white dwarf. However, the mass accretion releases a very large gravitational energy so that its thermal effect is significant.

The compression rate due to accretion, $\lambda_\rho \equiv (\partial \ln \rho/\partial t)_{M_r}$, is conveniently expressed as

$$\left.\begin{aligned} \lambda_\rho &\equiv (\partial \ln \rho/\partial t)_{M_r} = \lambda_\rho^{(M)} + \lambda_\rho^{(q)}, \\ \lambda_\rho^{(M)} &= (\partial \ln \rho/\partial \ln M)_q (d\ln M/dt), \\ \lambda_\rho^{(q)} &= -(\partial \ln \rho/\partial \ln q)_M (d\ln M/dt), \end{aligned}\right\} \qquad (6)$$

where the mass fraction $q \equiv M_r/M$ for a given Lagrangian shell decreases as M increases. The $\lambda_\rho^{(M)}$ term is due to the increase in density at fixed q as a result of the increase in M, while the $\lambda_\rho^{(q)}$ term shows the compression as the matter moves inward in q-space. In Figure 2, these rates λ_ρ, $\lambda_\rho^{(M)}$, and $\lambda_\rho^{(q)}$ are shown as a function of M_r for the initial stage of Case C ($M = 1.28\ M_\odot$ and $dM/dt = 7 \times 10^{-10} M_\odot yr^{-1}$). Since the change in the density distribution as a function of q is quite homologous,

$(\partial \ln \rho/\partial \ln M)_q$ and thus $\lambda_\rho^{(M)}$ is almost spacially uniform in the star as seen in Figure 2. In contrast, $\lambda_\rho^{(q)}$ is very large near the surface of the star because of the steep density gradient there (see Figure 1).

The energy release due to the $\lambda_\rho^{(M)}$ term can be estimated from equations (4) and (5) as

$$L_g^{(M)} \simeq \frac{kT}{\mu_I H} \lambda_\rho^{(M)} M \simeq 4 \times 10^{-2} L_\odot \left(\frac{M}{M_\odot}\right) \left(\frac{T}{3 \times 10^7 K}\right) \left(\frac{\lambda_\rho^{(M)}}{10^{-8} yr^{-1}}\right) \qquad (7)$$

where the uniform distribution of T and $\lambda_\rho^{(M)}$ is assumed. The compression rate $\lambda_\rho^{(M)}$ and thus $L_g^{(M)}$ are proportional to dM/dt. Also these values are functions of the white dwarf mass, M. In Figure 3, the stellar radius, R, and the central density, ρ_c, are given as a function of M for the models with the interior temperature of 3×10^7K. Since $d\ln \rho_c/dM$ is larger for larger M, especially near the Chandrasekhar limit, the compression rate at the center, $\lambda_{\rho,c} \equiv d\ln \rho_c/dt$, and the corresponding L_g [4] are increasing functions of M. In Figure 3, these functions are shown for $dM/dt = 7 \times 10^{-10} M_\odot yr^{-1}$.

The energy release by the $\lambda_\rho^{(q)}$ term can also be estimated as

$$L_g^{(q)} \simeq -\frac{k}{\mu_I H} \int_c^{surf.} T\, q\, d\ln \rho \frac{dM}{dt} \simeq 3 \times 10^{-2} L_\odot \left(\frac{T}{3 \times 10^7 K}\right) \left(\frac{dM/dt}{7 \times 10^{-10} M_\odot yr^{-1}}\right) \qquad (8)$$

which is comparable to $L_g^{(M)}$ and has a large effect on the temperature near the surface.

Since the initial luminosities, $L_{ph}^{(0)}$, of the white dwarfs for

cases A-F are in the range of 0.03 $L_\odot$ - 0.08 $L_\odot$, the compressional heating by ($L_g^{(M)} + L_g^{(q)}$) are significant as discussed below.

ii) Accretion with Moderate Rates (Cases A and B)

For cases A and B, the compressional heating rate is appreciably higher than the cooling rate of L_{ph}. Then the interior temperature rises as seen in Figure 4, where the changes in the temperature distribution are shown for several stages. Although the accretion begins from the same initial model (M_{C+O} = 1.08 $M_\odot$ at t = 0 yr), the thermal history of the interior depends sensitively on the accretion rate.

For Case A, a steep temperature peak appears near the surface as seen in the model at t = 1.7 x 10^5yr, because the compressional heating is more rapid near the surface than in the deep interior (see Figure 2) and because its timescale, λ_ρ^{-1}, is shorter than that of heat transport. During later phases, the rise in the temperature becomes slower due to the increasing L_{ph} and the inward heat transport. The temperature inversion persists until helium is ignited at t = 2.6 x 10^6yr.
For Case B, the accretion is ten times slower than in Case A and is slow enough for the interior to become almost isothermal due to heat diffusion. The temperature inversion in the early stage (t = 1.4 x 10^7yr) is negligibly small and disappears at t = 3 x 10^7yr. Moreover, more heat is lost from the star than in Case A while the same amount of helium has been accreted. Accordingly, the interior temperature is lower than in Case A. Such a dependence on the accretion rate is clearly seen in Figure 5,

where the evolutionary paths of the bottom of the accreted helium zone (hereafter denoted by subscript He and indicated by the filled circles) and the center of the white dwarf (indicated by the open circles) in the density - temperature plane are shown for cases A and B. As the mass of the accreted helium, ΔM_{He}, increases, T_{He} and ρ_{He} increase. If compared at the stage with the same ρ_{He}, T_{He} is lower for the slower accretion.

When ΔM_{He} reaches the value given in Table 1, helium is ignited off-center at a density of $\rho_{He}^{(ig)}$, also given in Table 1. The ignition point is defined by the time when the nuclear energy generation rate, ε_n, is equal to the energy loss rate by neutrinos, ε_ν, and radiation; i.e., $\varepsilon_n = \varepsilon_\nu + \partial L_r/\partial M_r$ where L_r denotes the radiative flux. The ignition was found to take place when the timescale of the temperature rise due to nuclear reaction, $\tau_n \equiv c_p T/\varepsilon_n$, is almost equal to 10^6yr. Here c_p denotes the specific heat. The corresponding ignition line is shown in ρ-T plane of Figure 5. For the slower accretion rate, the ignition of helium is delayed to a stage with higher ρ_{He}, i.e., larger ΔM_{He} because of the lower interior temperature. It should be noted that helium is ignited not at the base of the accreted envelope (i.e., $M_r = 1.080\ M_\odot$) but at the outer shell of $M_r = 1.086\ M_\odot$ for Case A because of the temperature inversion in the helium zone. In contrast, ignition occurs at the base of the helium envelope for Case B at $t = 7.2 \times 10^7$yr.

iii) Slow Accretion (Cases C-F)

For the cases with the accretion rate as slow as $dM/dt = (4\text{-}7) \times$

$10^{-10} M_\odot yr^{-1}$, the compressional heating rate, $(L_g^{(M)} + L_g^{(q)})$, is comparable to the photon cooling rate, L_{ph}. In Figure 6, the evolutionary paths of the bottom of the helium zone and the center are shown for cases C and F starting from the same initial model (t = 0 yr) but with different dM/dt. For both cases, the accretion is slow enough for the interior to become almost isothermal.

In the early stages of Case C, the cooling and the heating are almost balanced at $L_{ph} \sim 0.08\ L_\odot$, but later when $M > 1.33\ M_\odot$, the temperature increases because of the increasing compression rate of $\lambda_{\rho,c}$ (see Figure 3). For Case F, the photon cooling is always dominant over the gravitational energy release so that the temperature is decreasing during the accretion.

For Case C, T_{He} is lower than those in cases A and B so that the ignition of helium is delayed to the stage with $\rho_{He} = 2.4 \times 10^8 g\ cm^{-3}$ and $M = 1.402\ M_\odot$. This stage is just before the onset of carbon burning at the center. For Case F, in contrast, the central density becomes high enough to ignite carbon by the pycnonuclear reaction before ρ_{He} reaches the ignition line of helium. The structure lines at these ignition stages (dashed lines) and the ignition line of carbon given by $\tau_{C+C} = 10^6$ yr are shown in Figure 6.

Taam (1980b) suggested that accretion slower than $5 \times 10^{-10} M_\odot yr^{-1}$ leads to the ignition of carbon burning at the center prior to the helium ignition almost independently of the initial mass of M_{C+O}. However, he did not include the non-resonant regime of the 3α reaction in his computation. Since the resonant reaction rate depends much more sensitively

on the temperature than the non-resonant reaction rate does, the resonant rate drops sharply for $T < 5 \times 10^7$K despite the enhancement due to the strong screening. Therefore the temperature of the ignition line would be as high as $T \simeq 5 \times 10^7$K for $\rho \simeq 5 \times 10^6$g cm^{-3} if only the resonant reaction was taken into account. (If the non-resonant reaction had been included in Taam's (1980b) computation for his models with $dM/dt = 5 \times 10^{-10} M_\odot yr^{-1}$, he would have found the helium ignition to occur before carbon ignition as can be seen from his Table 3.)

Because of the weaker temperature dependence of the non-resonant reaction rate and the enhancement due to the strong screening, the ignition line of helium depends strongly on the density around $\rho \simeq (3\text{-}5) \times 10^6$g cm^{-3} as seen in Figure 6. This suggests that the mode of ignition (helium or carbon) depends strongly on the initial mass of the white dwarf M_{C+O} for relatively slow accretion rates.

In order to investigate this dependence, cases D and E were computed (see Table 1). The evolutionary paths in the (ρ_{He}, T_{He}) and the (ρ_c, T_c) plane, and the structure lines at the ignition stages are shown in Figure 7. For Case E with $dM/dt = 4 \times 10^{-10} M_\odot yr^{-1}$, the accretion begins from $M_{C+O} = 1.13\ M_\odot$, which is smaller than for Case F. It was then found that helium is ignited prior to carbon, just the opposite result to that for Case F. This is because, for the small M_{C+O}, the mass of the accreted helium, ΔM_{He}, can become large enough for ρ_{He} to reach the ignition line of helium before the white dwarf mass becomes large enough ($\sim 1.4\ M_\odot$) to ignite carbon. Similar comparison can also be made between cases C and D for which dM/dt again has the same (but larger) value, namely,

$7 \times 10^{-10} M_\odot yr^{-1}$. For Case C which has the smaller M_{C+O} of 1.28 $M_\odot$, helium ignition occurs before carbon ignition as described previously, while for Case D (M_{C+O} = 1.35 $M_\odot$) carbon ignition occurs first.

These cases demonstrate how changes in M_{C+O} can affect the nature of the triggering mechanism for the supernova explosion when dM/dt is fixed. It is found that, even for the very slow accretion, the carbon ignition occurs only for the white dwarfs whose M_{C+O} is larger than a certain critical mass M^*_{C+O}.

The critical mass, M^*_{C+O}, is mainly a function of dM/dt and is obtained in the following way. A crucial factor determining the ignition point is the temperature at the bottom of the helium zone and the center, i.e., T_{He} and T_c, which may depend on dM/dt and the initial models of the white dwarf (i.e., M_{C+O} and $T_c^{(0)}$). For most cases, the white dwarf is almost isothermal, i.e., $T_{He}/T_c \simeq (0.85 - 0.95)$ (see Table 1). Taam (1980b) found that the evolutionary paths in the $\rho_c - T_c$ plane for the models with the same dM/dt and M_{C+O} do not depend on $T_c^{(0)}$ at later stages. In the present investigation, models starting from different M_{C+O} were computed for the same dM/dt (Table 1). For both cases E and F with dM/dt = $4 \times 10^{-10} M_\odot yr^{-1}$, the central temperature reaches almost the same value of 1.7×10^7K at later stages with $\rho_c \simeq (0.8\text{-}1) \times 10^{10}$ g cm^{-3}. Also for dM/dt = $7 \times 10^{-10} M_\odot yr^{-1}$, $T_c \sim 3.7 \times 10^7$K is reached for both cases C and D when the flash is ignited.

These results show that T_c and the interior temperature distribution near the stage of carbon ignition depend mainly on dM/dt and only slightly on the initial conditions (i.e., M_{C+O} and $T_c^{(0)}$). This is because the

white dwarf evolves gradually towards the state with $L_{ph} \simeq L_g^{(M)} + L_g^{(q)}$ (see also FS). We note that, in the present computation, the temperature is somewhat lower than in FS and TM for the cases with the same dM/dt because the effect of Debye cooling was not included in FS and TM.

Once the ρ-T structure line at the stage of carbon ignition is given as a function of dM/dt, M^*_{C+O} can be estimated as follows. For dM/dt = $4 \times 10^{-10} M_\odot yr^{-1}$, the structure line crosses the ignition line of helium at $\rho_{He}^{(ig)} = 4.5 \times 10^6 g\ cm^{-3}$ which is the density at the shell with M_r = 1.17 $M_\odot$ in the model just at carbon ignition (Case F). This implies that $M^*_{C+O} \simeq 1.17\ M_\odot$ for this accretion rate. Similarly, M^*_{C+O} is estimated to be 1.28 $M_\odot$ for dM/dt = $7 \times 10^{-10} M_\odot yr^{-1}$. For other values of dM/dt, the temperature and the density distribution in the model just at the carbon ignition are obtained by interpolation and extrapolation; M^*_{C+O} is then obtained as a function of dM/dt. The line of $M_{C+O} = M^*_{C+O}$ in Figure 8 discriminates the mode of ignition in the (M_{C+O} - dM/dt) plane.

If the pycnonuclear reaction rate of carbon burning under the relaxed lattice approximation (Salpeter and Van Horn 1969) is adopted, the ignition density of carbon is lower than that based on the static lattice approximation by a factor of 1.3 (Figure 6). Correspondingly, the critical mass, M^*_{C+O}, is smaller as indicated by the dashed line in Figure 8.

c) Initiation of Thermonuclear Explosion

As described in the preceeding subsection, accretion onto C+O white dwarfs ignites various types of unstable nuclear burning depending on

dM/dt and M_{C+O}. In this subsection, I describe the transition phase from the ignition through the explosive stages.

i) Strong Helium Shell Flash

The progress of the unstable helium shell burning (flash) has been computed for cases A-C. Since the hydrostatic stages of the shell flashes under similar conditions have been investigated by FS and TM, I will focus on the transition from the hydrostatic through hydrodynamic phases of the flash.

Because of strong electron degeneracy, the temperature of the burning shell, T_{He}, rises as shown by the solid lines in Figures 5 and 6. A convective zone develops, and the superadiabatic temperature gradient increases as ϵ_n increases. When T_{He} reaches the stage with $\tau_n \simeq 100\tau_d$ ($\tau_d = (24\pi G\rho)^{-1/2}$ is the dynamical timescale), convection can transport only a negligible fraction of the nuclear energy generation. The dashed lines in Figure 5 snows the structure lines of the white dwarfs in ρ-T plane when such a blocking of heat occurs. Afterwards the progress of the flash is confined to a very thin shell and T_{He} rises quickly.

Soon T_{He} reaches a deflagration temperature, T_{def}, defined by $\tau_n = \tau_d$ as indicated in Figures 5 and 6. The rapid nuclear energy release increases the pressure; the overpressure ΔP, i.e., the excess of pressure over that required for the hydrostatic equilibrium, develops. In other words, the hydrodynamic phase begins. The effect of the inertial force delays the expansion of the burning shell and keeps T_{He} rising (Sugimoto

1964). The ratio $\Delta P/P$ increases from 8×10^{-4} to 0.1 (Case A), from 4×10^{-4} to 3×10^{-2} (Case B), and from 5×10^{-5} to 7×10^{-3} (Case C) during the evolution from the stage with $T_{He} = T_{def}$ to $T_{He} = 2\ T_{def}$; the thermal overpressure is larger for the lower density because of lower electron-degeneracy. Ultimately, the increasing $\Delta P/P$ results in the formation of a shock front and an off-center detonation wave as will be described in Paper II (see preliminary reports by Nomoto (1980a,b)).

As has been shown by Nomoto and Sugimoto (1977) for the off-center flash in helium white dwarfs and by FS and TM for C+O white dwarfs, the accretion at the higher rate considered here (i.e., $dM/dt \gtrsim 4 \times 10^{-8} M_\odot yr^{-1}$) ignites the helium at such a low density, $\rho_{He}^{(ig)} < 10^6 g\ cm^{-3}$, that the resultant helium shell flash is too weak to induce any dynamical effects. Therefore, accretion can trigger an off-center helium detonation only in a restricted region of the $(dM/dt, M_{C+O})$ plane, as shown in Figure 8.

ii) Carbon Flash

The progress of the carbon burning for Case F is shown in Figure 6. Since the pycnonuclear reaction rate depends very weakly on the temperature, the central temperature rises relatively slowly with a timescale of $dt/d\ln T_c \simeq 10^5 yr$. During such a slow rise in T_c, the central density continues to increase due to the accretion, which in turn increases the reaction rate. For $T > 5 \times 10^7 K$, the carbon burning changes from the pycnonuclear regime to the thermonuclear regime so that the thermal runaway is accelerated (see also Taam 1980b), leading to the carbon deflagration

supernova (Nomoto et al. 1976; Nomoto 1980a,b). This type of supernova explosion occurs for $M_{C+O} \geq M^{*}_{C+O}$ in the (dM/dt, M_{C+O}) plane of Figure 8.

The carbon deflagration supernova is also triggered by rapid accretion in the region of $dM/dt \gtrsim 4 \times 10^{-6} M_{\odot} yr^{-1}$ in Figure 8. As mentioned above, the helium shell flashes for such an accretion are very weak and so will recur many times to increase the mass of the C+O white dwarf. Such an evolution is very similar to the growth of the degenerate C+O core in red giant stars, although further investigation is needed on the mixing of hydrogen-rich material into the helium-burning convective zone which might lead to the hydrogen flash and s-process nucleosynthesis and make the evolution more complex (FS; TM; Iben 1981). Finally carbon will be ignited at the center of the white dwarf, which will lead to the carbon deflagration supernova (Nomoto et al. 1976).

IV. CONCLUSION

Based on the results of the preceding section, the relationship between the triggering mechanisms of SN I and the conditions in the binary system is summarized in the (M_{C+O} - dM/dt) plane (Figure 8). SN I are triggered by either the off-center detonation of helium for slow and intermediate accretion rates or the central carbon flash for slow and rapid accretion rates. Such a variation in the mode of ignition may cause some variations among SN I (Barbon et al. 1973; Paczynski 1977; Branch 1981).

This diagram is different from Taam's (1980b) preliminary one in the part for slow accretion ($dM/dt < 1 \times 10^{-9} M_\odot yr^{-1}$) where both off-center detonation and carbon deflagration are possible; the domains in the (M_{C+O} - dM/dt) plane corresponding to the two triggering mechanisms are separated by the line for $M_{C+O} = M^*_{C+O}$. When the carbon is ignited by the slow accretion for the case with $M_{C+O} > M^*_{C+O}$, the white dwarf has a thick helium zone of mass $\Delta M_{He} = 1.40\ M_\odot - M_{C+O} \leq 1.40\ M_\odot - M^*_{C+O}$. The upper bounds on the mass of the helium zone are 0.25 $M_\odot$ and 0.27 $M_\odot$ for the pycnonuclear reaction of carbon under the static and relaxed lattice approximation, respectively. This is in contrast to the case of carbon ignition under rapid accretion in which ΔM_{He} should be smaller than $6 \times 10^{-4} M_\odot$ in order to avoid the occurence of helium detonation (FS). The presence of such a thick helium zone may also cause the variations among SN I. The present finding implies that the initial mass function of the white dwarfs in close binary systems (Webbink 1980) is important for estimating the frequency of each type of supernova.

V. DISCUSSION

In Figure 8, dM/dt denotes the accretion rate of helium which is a result of hydrogen shell burning or a direct transfer of helium from the companion star. When the helium is produced by the recurring hydrogen shell flashes, dM/dt is not necessarily the same as the accretion rate of hydrogen-rich matter, dM_H/dt, from the companion star. In the following, I will discuss several modes of building up of the helium zone.

a) Direct Transfer of Helium

During the evolution in some binary systems, it is possible that helium is directly transfered from the companion star to the white dwarf: If the companion star is a helium star in the mass range of 1.0 - 2.5 $M_\odot$, its helium envelope expands to a red giant size when the degenerate C+O core (Paczyński 1971) or O+Ne+Mg core (Nomoto 1980a,b) is formed. Then the helium envelope overflows the Roche lobe and accretes onto the white dwarf rather rapidly. Also the emission of gravitational waves in the compact binary system could drive the transfer of helium from the degenerate helium dwarf companion to the white dwarf. Although the observed examples of such compact binary systems as HZ-29 (Faulkner, Flannery, and Warner 1972) and G61-29 (Nather, Robinson, and Stover 1981) have too small a mass for the system to evolve into a SN I, more massive systems could exist.

In such a direct accretion of helium, very rapid accretion is possible.

If the accretion rate of helium, dM/dt, is higher than a certain critical rate, $(dM/dt)_{RHe}$, given in equation (9) below, the accreted helium will be piled up to form a red giant like envelope after a very weak flash as also shown for the rapid accretion of hydrogen-rich matter (Nomoto, Nariai, and Sugimoto 1979). This critical rate corresponds to the growth rate of the mass of the C+O core through helium shell burning at the bottom of a helium envelope of red-giant size. Applying Uus's (1970) result for the helium star of 1.5 - 3.0 $M_\odot$, this rate is given by

$$(dM/dt)_{RHe} = 7.2 \times 10^{-6} (M_{C+O}/M_\odot - 0.60)\ M_\odot yr^{-1}, \qquad (9)$$

for $0.75 \leq M_{C+O}/M_\odot \leq 1.38$ and shown in Figure 8. The upper limit for the accretion rate of helium is determined by the Eddington limit, $(dM/dt)_{EHe}$, and is also shown in Figure 8.

Formation of an extended helium envelope will lead to the phase of double degenerate cores embedded in the common helium envelope. More investigation is needed to clarify whether such a system evolves into twin white dwarfs by blowing off the envelope (Taam, Bodenheimer, and Ostriker 1978) or into a supernova triggered by the collision of the cores (Sparks and Stecher 1974). If the latter case were to occur, a peculiar SN I might result. The outcome for the accretion of $dM/dt < (dM/dt)_{RHe}$ have already been summarized in Figure 8.

b) Hydrogen Shell Burning

When the hydrogen-rich matter accretes onto the white dwarf, hydrogen shell burning is ignited. How much mass of accreted hydrogen is processed into helium depends on the type and the strength of the hydrogen shell burning and thus depends sensitively on the accretion rate of hydrogen-rich matter, dM_H/dt. This is analogous to the case of helium shell burning discussed in the preceding subsection and summarized as follows (see Sugimoto and Miyaji 1980 for a review).

(1) Rapid Accretion Forming a Red Giant Like Envelope: When the accretion is as rapid as $dM_H/dt \gtrsim (dM/dt)_{RH}$, the accreted matter forms a red giant like envelope (Nomoto et al. 1979). This critical rate, $(dM/dt)_{RH}$, corresponds to the growth rate of the degenerate core in red giant stars due to the hydrogen shell burning. Paczyński's (1970) core mass to luminosity relation assuming a hydrogen abundance of $X = 0.7$ gives

$$(dM/dt)_{RH} = 8.5 \times 10^{-7}(M/M_\odot - 0.52)\ M_\odot yr^{-1}, \qquad (10)$$

for $0.60 \leq M/M_\odot \leq 1.39$, where the core mass is replaced by the white dwarf mass M. In Figure 9, $(dM/dt)_{RH}$ and the Eddington limit, $(dM/dt)_{EH}$, for hydrogen are shown. The red giant like envelope of the white dwarf can cause various further evolution of the interacting binary as mentioned for the rapid accretion of helium; if the common hydrogen-rich envelope is blown off by spiraling of the white dwarf into the companion star (Taam et al. 1978), a helium companion star would be left, and the resultant

system, having a relatively short period, could evolve into a phase of direct accretion of helium onto the white dwarf.

(2) Steady Burning: For the accretion rate in the range of $0.4\ (dM/dt)_{RH} \lesssim dM_H/dt < (dM/dt)_{RH}$, the hydrogen shell burning is stable (Paczyński and Żytkow 1978; Sion, Acierno, and Tomczyk 1979; Sienkiewicz 1980). Such hydrogen burning processes the accreted matter into helium at a rate of $dM/dt = dM_H/dt$.

(3) Recurrence of Flashes: When the accretion rate is slower than $0.4\ (dM/dt)_{RH}$, the hydrogen shell burning becomes unstable and flashes. How much of the accreted mass is processed into helium without escaping from the white dwarf depends on the strength of the flash and thus on dM_H/dt. For higher dM_H/dt, the mass of the accreted matter, ΔM_H, at the time of hydrogen ignition is smaller as shown in Figure 9. Here the value of ΔM_H is taken from the models computed by Nariai and Nomoto (1979) where the compressional heating due to accretion is just balanced with the cooling due to heat conduction; such a condition is realized after many flash cycles.

In general, smaller ΔM_H and smaller M lead to a weaker flash because of the lower pressure at the flashing shell (Sugimoto et al. 1979). When ΔM_H is sufficiently small, the flash gives rise to no mass ejection nor appreciable expansion so that the white dwarf appears as an EUV nova (Shara, Prialnik and Shaviv 1978). Sion et al. (1979) also found that such weak flashes occur in the models with $M = 1.2\ M_\odot$ and $dM_H/dt = 2 \times 10^{-7} - 10^{-8} M_\odot yr^{-1}$. Therefore, a large portion of the accreted matter will be processed into helium for accretion as rapid as $dM_H/dt \simeq 2 \times 10^{-7}$ -

$10^{-8} M_\odot yr^{-1}$ (see also Nomoto 1980c).

For the slower accretion, the flash is stronger because of larger ΔM_H. It is still likely that a finite amount of helium is left even when a nova-like explosion occurs, so that the helium zone can grow at a rate of dM/dt which is slower than dM_H/dt. One might worry that the companion star could not supply enough hydrogen to lead to SN I if dM/dt is much smaller than dM_H/dt by, say, a factor of 10. It depends on the parameters in the binary system. If the initial white dwarf is as massive as $M_{C+O} \simeq 1.3 - 1.4\ M_\odot$, the accumulation of at least $10^{-2} - 10^{-3} M_\odot$ helium can trigger the helium detonation (FS). Therefore, the accretion of in total $0.1 - 0.01\ M_\odot$ hydrogen is enough to give rise to SN I. If the companion star would lose all its hydrogen-rich envelope before a SN I is triggered, the accretion would stop and the white dwarf would cool again; as a result of further evolution, however, it could occur that the companion star would transfer helium onto the white dwarf driven by the expansion of the helium envelope or by the emission of the gravitational waves.

(4) Diffusion for Slow Accretion: When the accretion rate is as slow as $10^{-10} - 10^{-11} M_\odot yr^{-1}$, the accretion continues as long as $\tau_{acc} \simeq \Delta M_H/(dM_H/dt) \simeq 10^6 - 10^7$yr before the ignition of the hydrogen shell burning as estimated from Figure 9. Starrfield, Truran, and Sparks (1981) suggested that the CNO nuclei could diffuse out of the accreted matter in such a long τ_{acc}. If it leads to stable burning by the proton-proton chain, a helium zone will be built up at a rate of $dM/dt = dM_H/dt$. However, more quantitative investigation of the diffusion process during the accretion is needed.

The above discussion in points (1)-(4) shows that SN I from accreting white dwarfs can occur over a rather wide range of accretion rates. If other conditions are the same, more rapid accretion triggers SN I more frequently because of the shorter accretion time. In this respect, the investigation of the connection between SN I and the symbiotic stars might be interesting, because Paczyński and Rudak (1980) suggested that some symbiotic stars may consist of white dwarfs on which hydrogen is burning steadily or weak flashes are occurring. Such weak hydrogen flashes recur many times before a SN I is triggered; the number of flashes is estimated from the mass ratio between ΔM_{He} at the initiation of flash (helium or carbon) and the average value of ΔM_H during the growth of M assuming negligible mass ejection. The value of ΔM_H gives an upper limit for the hydrogen mass when a SN I occurs. Their smallness compared with M is consistent with the hydrogen-deficiency in SN I.

It is also important to investigate various evolutionary paths of interacting binaries leading to a phase of direct transfer of helium from a companion star to the white dwarf (see reviews by Webbink 1979 and by Tutukov 1980), e.g., the evolution after the contact system is formed and after the recurrent nova explosions finally cease as discussed above in point (1) and (3).

I am grateful to Prof. D. Sugimoto for stimulating discussions and to Dr. M.Y. Fujimoto for his help in the initial stages of this investigation. It is a pleasure to thank Drs. W. M. Sparks and A. V. Sweigart for the reading of the manuscript, useful comments, and encouragement during my stay at NASA-GSFC, and to H. Nomoto for preparation of the manuscript. This work has been supported in part by NRC-NASA Research Associateships in 1979-1981.

TABLE 1

Initial and Ignition Models [a]

Initial Models

Case	A	B	C	D	E	F
M_{C+O} ($M_\odot$)	1.08	1.08	1.28	1.35	1.13	1.28
dM/dt ($M_\odot yr^{-1}$)	$3x10^{-8}$	$3x10^{-9}$	$7x10^{-10}$	$7x10^{-10}$	$4x10^{-10}$	$4x10^{-10}$
$L_{ph}^{(0)}$ ($L_\odot$)	0.03	0.03	0.07	0.08	0.03	0.07
log $T_c^{(0)}$ (K)	7.37	7.37	7.42	7.42	7.34	7.42
log $\rho_c^{(0)}$ (g cm^{-3})	7.76	7.76	8.59	9.14	7.92	8.59

Ignition Models

Case	A	B	C	D	E	F
Ignited Fuel	He	He	He	C	He	C
t (yr)	$2.60x10^6$	$7.77x10^7$	$1.74x10^8$	$7.57x10^7$	$6.68x10^8$	$3.03x10^8$
ΔM_{He} ($M_\odot$)	0.078	0.233	0.122	0.053	0.267	0.121
log T_{He} (K)	7.90[b]	7.77	7.53	7.49	7.20	7.16
log ρ_{He} (g cm^{-3})	6.44[b]	7.56	8.38	7.93	8.67	8.36
log T_c (K)	7.53	7.80	7.58	7.56	7.23	7.22
log ρ_c (g cm^{-3})	8.02	8.82	10.04	10.08	9.90	10.03

a Subscripts He and c denote the bottom of the helium envelope and the center, respectively.

b For Case A, ρ_{He} and T_{He} correspond to the values at the ignited shell which does not coincide with the bottom of the helium envelope.

REFERENCES

Alastuey, A. and Jancovici, B. 1978, Ap. J., 226, 1034.

Appenzeller, I. 1970, Astr. Ap., 5, 355.

Arnett, W.D. 1979, Ap. J. (Letters), 230, L37.

Axelrod, T.S. 1980a, in Type I Supernovae, ed. J.C. Wheeler (Austin: University of Texas), P.80.

Axelrod, T.S. 1980b, Ph. D. Thesis, University of California at Santa Cruz.

Barbon, R., Ciatti, F., and Rosino, L. 1973, Astr. Ap., 25, 241.

Barnes, C.A. 1980, Preprint (OAP-593), Lectures at the International School of Nuclear Physics, Erice, Italy.

Branch, D. 1981, Ap. J., in press.

Cameron, A.G.W. 1959, Ap. J., 130, 916.

Chevalier, R.A. 1981a, Fund. of Cosmic Phys., 7, 1.

Chevalier, R.A. 1981b, Ap. J., 246, 267.

Clayton, D.D. 1968, Principles of Stellar Evolution and Nucleosynthesis (New York: McGraw-Hill).

Colgate, S.A., Petschek, A.G., and Kriese, J.T. 1980, Ap. J. (Letters), 237, L81.

Faulkner, J., Flannery, B.P., and Warner, B. 1972, Ap. J. (Letters), 175, L79.

Finzi, A. and Wolf, W.A. 1967, Ap. J., 150, 115.

Fowler, W.A., Caughlan, G.R., and Zimmerman, B.A. 1975, Ann. Rev. Astr. Ap., 13, 69.

Fujimoto, M.Y. and Sugimoto, D. 1979, in IAU Colloquium No.53, White Dwarfs and Variable Stars, ed. H.M. Van Horn and V. Weidemann (Rochester: University of Rochester), p.285.

Fujimoto, M.Y. and Sugimoto, D. 1981, preprint.

Gravoske, H.C., DeWitt, H.E., Grossman, A.S., and Cooper, M.S. 1973, Ap. J., 181, 457.

Iben, I. Jr. 1975, Ap. J., 196, 525.

Iben, I. Jr. 1981, Ap. J., 243, 987.

Itoh, N., Totsuji, H., and Ichimaru, S. 1977, Ap. J., 218, 477; erratum 1978, Ap. J., 220, 742.

Itoh, N., Totsuji, H., Ichimaru, S., and DeWitt, H.E. 1979, Ap. J., 234, 1079; erratum 1980, Ap. J., 239, 415.

Kirshner, R.P. and Oke, J.B. 1975, Ap. J., 200, 574.

Lasher, G. 1975, Ap. J., 201, 194.

Maza, J. and van den Bergh, S. 1976, Ap. J., 204, 519.

Mazurek T.J. 1973, Ap. Space Sci., 23, 365.

Mazurek, T.J. and Wheeler, J.C. 1980, Fund. of Cosmic Phys., 5, 193.

Meyerott, R.E. 1980, Ap. J., 239, 257.

Nariai, K. and Nomoto, K. 1979, in IAU Colloquium No.53, White Dwarfs and Variable Degenerate Stars, ed. H.M. Van Horn and V. Weidemann (Rochester: University of Rochester), p.525.

Nariai, K., Nomoto, K., and Sugimoto, D. 1980, Publ. Astr. Soc. Japan, 32, 473.

Nather, R.E., Robinson, E.L., and Stover, R.J. 1981, Ap. J., 244, 269.

Nomoto, K. 1980a, in Type I Supernovae, ed. J.C. Wheeler (Austin: University of Texas), p.164.

Nomoto, K. 1980b, in IAU Symposium No.93, Fundamental Problems in the Theory of Stellar Evolution, ed. D. Sugimoto, D.Q. Lamb, and D.N. Schramm (Dordrecht: Reidel), p.295.

Nomoto, K. 1980c, Space Sci. Rev., 27, 563.

Nomoto, K., Nariai, K., and Sugimoto, D. 1979, Publ. Astr. Soc. Japan, 31, 287.

Nomoto, K. and Sugimoto, D. 1977, Publ. Astr. Soc. Japan, 29, 765.

Nomoto, K., Sugimoto, D., and Neo, S. 1976, Ap. Space Sci., 39, L37.

Oke, J.B. and Searle, L. 1974, Ann. Rev. Astr. Ap., 12, 315.

Paczyński, B. 1970, Acta Astr., 20, 47.

Paczyński, B. 1971, Acta Astr., 21, 1.

Paczyński, B. and Rudak, B. 1980, Astr. Ap., 82, 349.

Paczyński, B. and Żytkow, A.N. 1978, Ap. J., 222, 604.

Pollock, E.L. and Hansen, J.P. 1973, Phys. Rev. A, 8, 3110.

Pskovskii, Y.P. 1977, Sov. Astr., 21, 675.

Richtmeyer, R.D. and Morton, K.W. 1967, Difference Methods for Initial Value Problems (2d ed.; New York: Interscience).

Salpeter, E.E. 1961, Ap. J., 134, 669.

Salpeter, E.E. and Van Horn, H.M. 1969, Ap. J., 155, 183.

Sampson, D.H. 1961, Ap. J., 134, 482.

Shara, M.M., Prialnik, D., and Shaviv, G. 1978, Astr. Ap., 61, 363.

Sienkiewicz, R. 1980, Astr. Ap., 85, 295.

Sion, E.M., Acierno, M.J., and Tomczyk, S. 1979, Ap. J., 230, 832.

Sparks, W.M. and Stecher, T.P. 1974, Ap. J., 188, 149.

Starrfield, S., Truran, J.W., and Sparks, W.M. 1981, Ap. J. (Letters), 243, L27.

Sugimoto, D. 1964, Prog. Theor. Phys., 32, 703.

Sugimoto, D. 1970, Ap. J., 159, 619.

Sugimoto, D., Fujimoto, M.Y., Nariai, K., and Nomoto, K. 1979, in IAU Colloquium No.53, White Dwarfs and Variable Degenerate Stars, ed. H.M. Van Horn and V. Weidemann (Rochester: University of Rochester), p.280.

Sugimoto, D. and Miyaji, S. 1980, in IAU Symposium No.93, Fundamental Problems in the Theory of Stellar Evolution, ed. D. Sugimoto, D.Q. Lamb, and D.N. Schramm (Dordrecht: Reidel), in press.

Sugimoto, D. and Nomoto, K. 1975a, Publ. Astr. Soc. Japan, 27, 197.

Sugimoto, D. and Nomoto, K. 1975b, Sci. Pap. Coll. Gen. Educ. Univ. Tokyo, 25, 109.

Sugimoto, D. and Nomoto, K. 1980, Space Sci. Rev., 25, 155.

Taam, R.E. 1980a, Ap. J., 237, 142.

Taam, R.E. 1980b, Ap. J., 242, 749.

Taam, R.E., Bodenheimer, P., and Ostriker, J.P. 1978, Ap. J., 222, 269.

Tammann, G.A. 1974, in Supernovae and Supernova Remnants, ed. C.B. Cosmovici (Dordrecht: Reidel), p.155.

Tutukov, A.V. 1980, in IAU Symposium No.93, Fundamental Problems in the Theory of Stellar Evolution, ed. D. Sugimoto, D.Q. Lamb, and D.N. Schramm (Dordrecht: Reidel), in press.

Unno, W. 1967, Publ. Astr. Soc. Japan, 19, 140.

Uus, U. 1970, Nauch. Inform. Akad. Nauk USSR, 17, 25.

Van Horn, H.M. 1969, in Low-Luminosity Stars, ed. S.S. Kumar (New York: Gordon and Breach), p.297.

Van Horn, H.M. 1971, in IAU Symposium No.42, White Dwarfs, ed. W.J. Luyten (Dordrecht: Reidel), p.97.

Weaver, T.A., Axelrod, T.S., and Woosley, S.E. 1980, in Type I Supernovae, ed. J.C. Wheeler (Austin: University of Texas), p.113.

Webbink, R.F. 1979, in IAU Colloquium No.53, White Dwarfs and Variable Degenerate Stars, ed. H.M. Van Horn and V. Weidemann (Rochester: University of Rochester), p.426.

Webbink, R.F. 1980, Bull. AAS., 12, 848.

Wheeler, J.C. 1978, Ap. J., 225, 212.

Wheeler, J.C. 1981, Reports on Progress in Physics, in press.

Whelan, J. and Iben, I. Jr. 1973, Ap. J., 186, 1007.

Woosley, S.E., Weaver, T.A., and Taam, R.E. 1980, in Type I Supernovae, ed. J.C. Wheeler (Austin: University of Texas), p.96.

Yokoi, K., Neo, S., and Nomoto, K. 1979, Astr. Ap., 77, 210.

FIGURE CAPTIONS

Figure 1: Changes in the density distribution in the accreting white dwarfs are shown for cases A and C. The interior matter is compressed to higher densities as the white dwarf mass, M_{WD}, increases. The accretion starts at an initial mass of $M_{WD} = 1.080\ M_\odot$ (Case A) and $1.280\ M_\odot$ (Case C). Helium is ignited at $M_{WD} = 1.158\ M_\odot$ (Case A) and $1.402\ M_\odot$ (Case C). Open and filled circles indicate the center of the white dwarf and the bottom of the accreted helium zone, respectively.

Figure 2: The rates of compression due to mass accretion onto the white dwarf are shown for the initial stage of Case C ($M_{WD} = 1.28\ M_\odot$ and $dM/dt = 7 \times 10^{-10} M_\odot yr^{-1}$). These rates are difined by $\lambda_\rho^{(M)} \equiv (\partial \ln \rho/\partial \ln M)_q\ (d\ln M/dt)$, $\lambda_\rho^{(q)} \equiv -(\partial \ln \rho/\partial \ln q)_M\ (d\ln M/dt)$, and $\lambda_\rho = \lambda_\rho^{(M)} + \lambda_\rho^{(q)}$.

Figure 3: The central density, ρ_c, and the stellar radius, R, for white dwarfs with a central temperature $T_c = 3 \times 10^7 K$ are shown as a function of the white dwarf mass M_{WD}. The compression rate by accretion, $\lambda_{\rho,c} \equiv (d\ln \rho_c/dM)(dM/dt)$ and the corresponding gravitational energy release $L_g^{(M)}$ for $dM/dt = 7 \times 10^{-10} M_\odot yr^{-1}$ and $T_c = 3 \times 10^7 K$ are given as a function of M_{WD}.

Figure 4: Changes in the temperature distribution for cases A and B are shown. The initial model (t = 0 yr; M_{WD} = 1.08 $M_\odot$) at the onset of accretion are the same for both cases A and B. At the stages of t = 2.6 x 10^6yr for Case A and t = 7.2 x 10^7yr for Case B, helium ignition occurs.

Figure 5: Evolutionary paths (solid lines) of the density and temperature at the bottom of the accreted helium zone (filled circle) and at the center of the white dwarf (open circle) for cases A (dM/dt = 3 x $10^{-8}M_\odot yr^{-1}$) and B (3 x $10^{-9}M_\odot yr^{-1}$). For Case A, the rise in temperature after the helium ignition is shown for the shell with maximum temperature which does not coincide with the bottom of the helium layer (see text). Dashed lines show the structure of the white dwarfs from the center to the surface at the stages when the accretion begins (t = 0 yr) and when the heat blockage occurs in the helium-burning shell. Dotted lines are the ignition lines for helium and carbon defined by $\tau_n = 10^6$yr and $\epsilon_n = \epsilon_\nu$. The deflagration temperature for helium defined by $\tau_{He} = \tau_d$ is also shown by dotted line.

Figure 6: Same as Figure 5 but for cases C (dM/dt = 7 x $10^{-10}M_\odot yr^{-1}$) and F (4 x $10^{-10}M_\odot yr^{-1}$). The structure lines (dashed lines) are shown for the initial stage (t = 0 yr) and for the stage when helium (Case C) or carbon (Case F) are ignited. The ignition lines indicated by (S) and (R) for carbon burning (dash-dotted line) correspond

to the pycnonuclear reaction under the static and relaxed lattice approximation, respectively.

Figure 7: Same as Figures 4 and 5 but for Cases D and E.

Figure 8: Relationship between the triggering mechanisms for Type I supernovae and the conditions in the binary system, i.e., the initial mass of the white dwarf, M_{C+O}, and the accretion rate of helium, dM/dt. Filled circles show cases A-F computed in the present study. Solid and dashed lines for the critical mass, M^{*}_{C+O}, correspond to the pycnonuclear reaction of carbon under the static and relaxed lattice approximation, respectively. $(dM/dt)_{RHe}$ corresponds to the growth rate of the C+O core in the red giant-size helium star, and $(dM/dt)_{EHe}$ shows the Eddington's critical rate for helium. For $(dM/dt)_{RHe} \leq dM/dt \leq (dM/dt)_{EHe}$, a red giant-like helium envelope is formed.

Figure 9: Types and strengths of the hydrogen shell burning are shown as a function of accretion rate of hydrogen-rich matter, dM_H/dt, and the white dwarf mass, M_{WD}. $(dM/dt)_{EH}$ is the Eddington's critical rate for hydrogen and $(dM/dt)_{RH}$ corresponds to the growth rate of the degenerate core in red giant stars. For $(dM/dt)_{RH} \leq dM_H/dt \leq (dM/dt)_{EH}$, the accretion leads to the formation of a red giant-like envelope. For $0.4\ (dM/dt)_{RH} \lesssim dM_H/dt < (dM/dt)_{RH}$, the resultant hydrogen shell burning is stable and steady. For slower accretion, the hydrogen shell burning becomes unstable and flashes. ΔM_H is the mass of the accreted hydrogen-rich envelope at the ignition of hydrogen (see text).

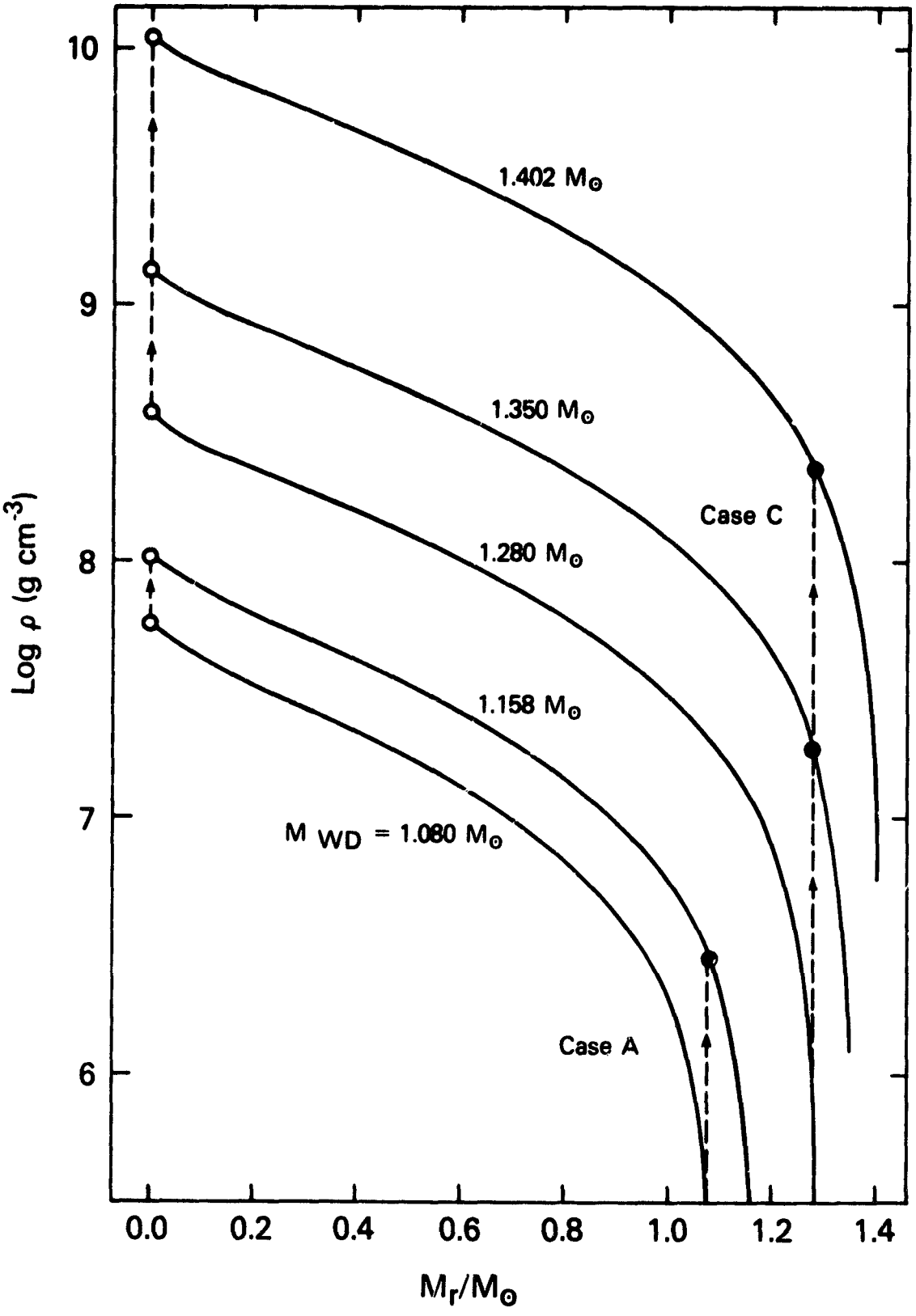
10
9
8
7
6
Log ρ (g cm^{-3})
1.402 M$_\odot$
1.350 M$_\odot$
1.280 M$_\odot$
1.158 M$_\odot$
M WD = 1.080 M$_\odot$
Case C
Case A
0.0
0.2
0.4
0.6
0.8
1.0
1.2
1.4
M$_r$/M$_\odot$

Figure 1

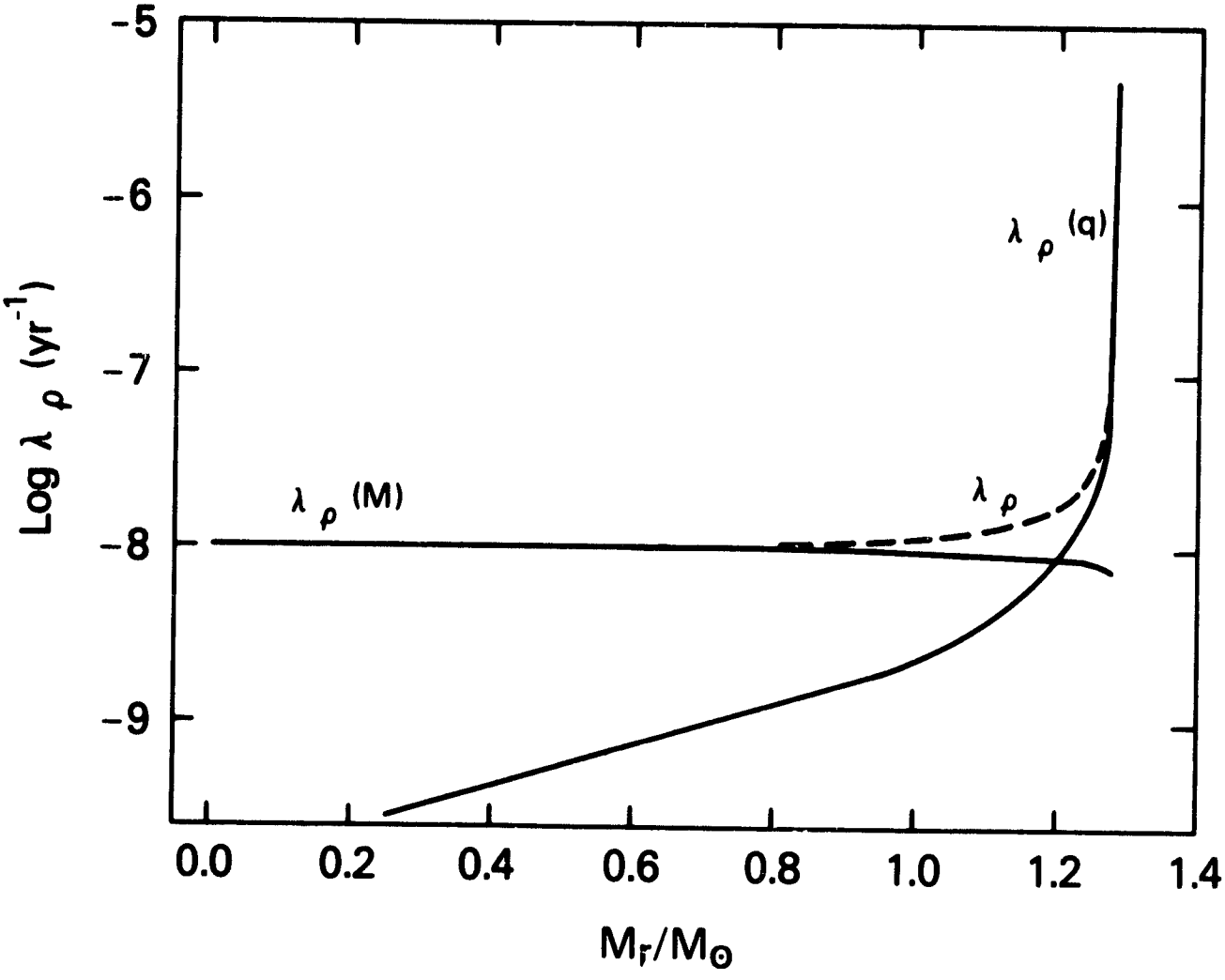

Figure 2

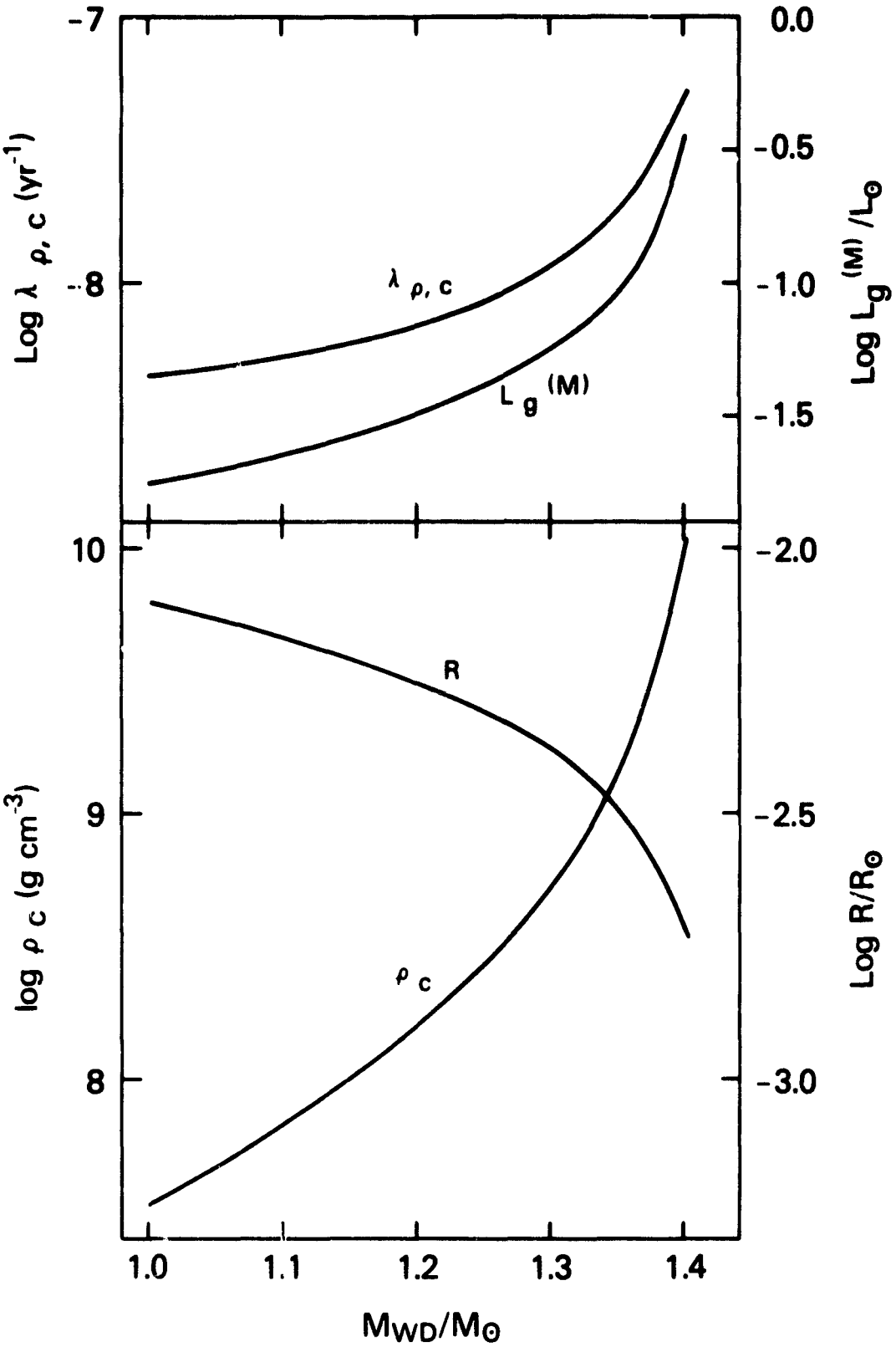
-7
-8
0.0
-0.5
-1.0
-1.5
Log λ ρ, c (yr-1)
λ ρ, c
L g (M)
Log Lg(M) /L⊙
10
9
8
-2.0
-2.5
-3.0
R
ρ c
log ρ c (g cm-3)
Log R/R⊙
1.0
1.1
1.2
1.3
1.4
MWD/M⊙

Figure 3

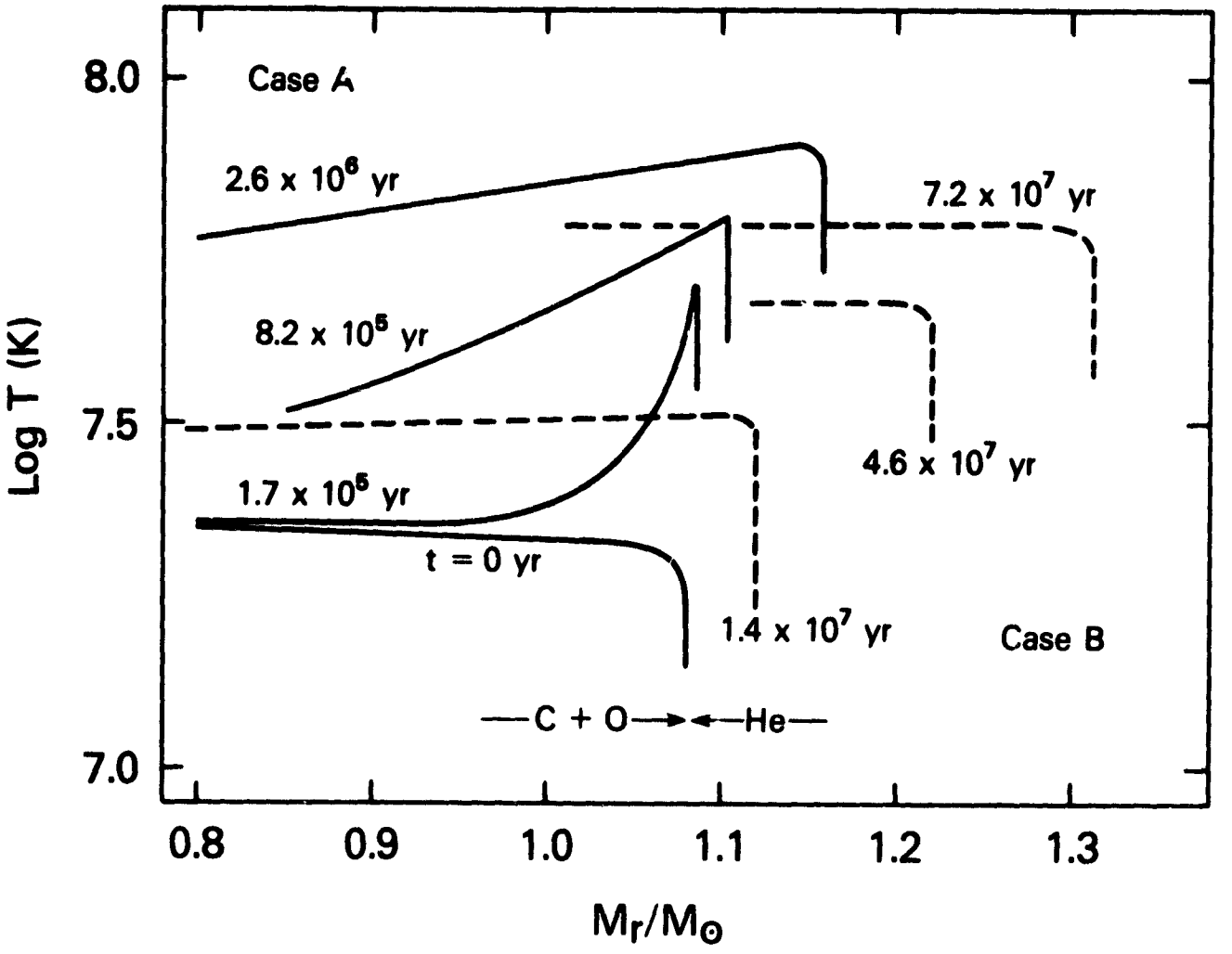
8.0
7.5
7.0
Log T (K)
Case A
2.6 x 10^6 yr
8.2 x 10^5 yr
1.7 x 10^5 yr
t = 0 yr
7.2 x 10^7 yr
4.6 x 10^7 yr
1.4 x 10^7 yr
Case B
—C + O→←He—
0.8
0.9
1.0
1.1
1.2
1.3
Mr/M⊙

Figure 4

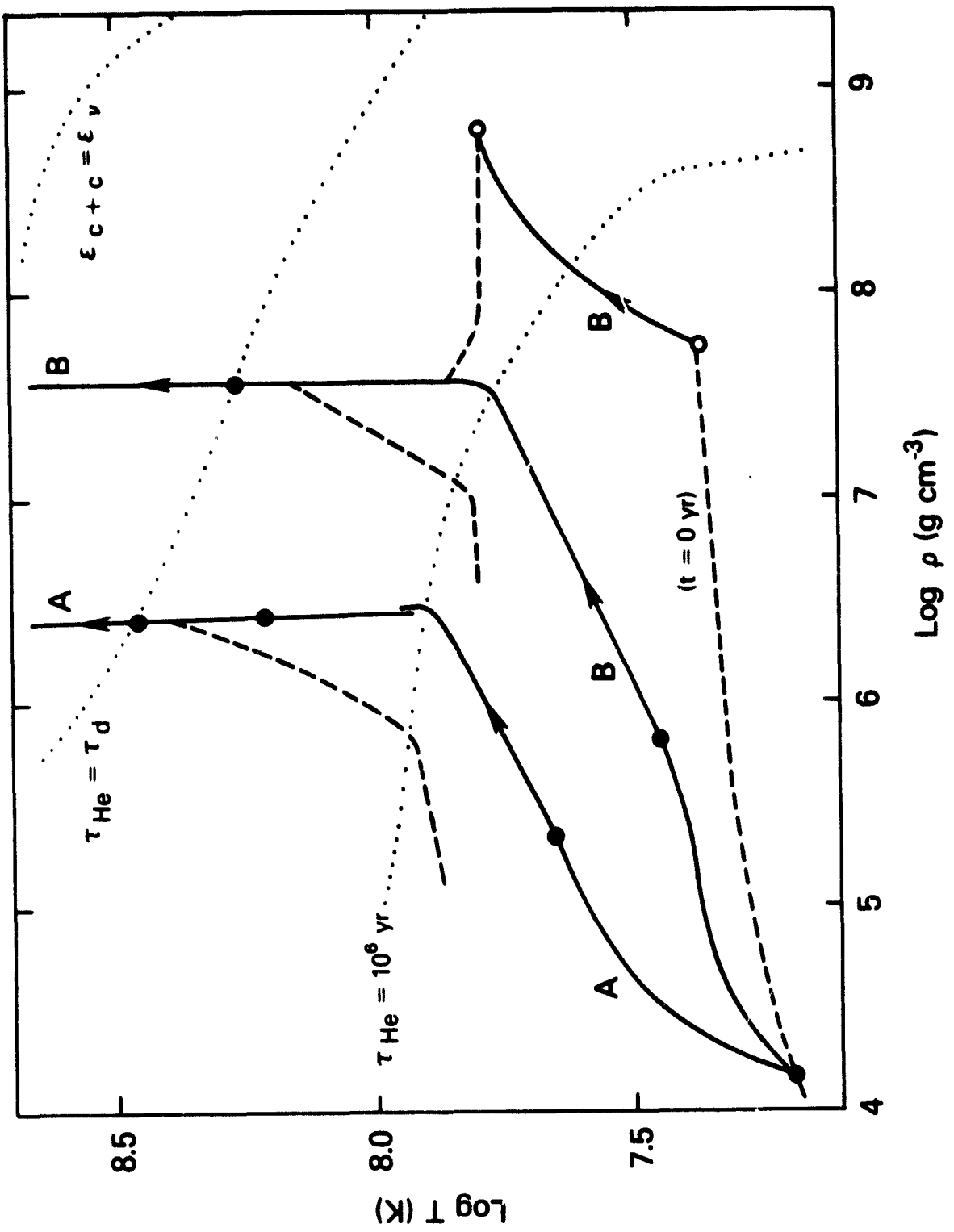
Log T (K)
8.5
8.0
7.5
Log ρ (g cm^{-3})
4
5
6
7
8
9
A
B
B
A
B
$\tau_{He} = \tau_d$
$\tau_{He} = 10^6$ yr
(t = 0 yr)
$\epsilon_{c+c} = \epsilon_\nu$

Figure 5

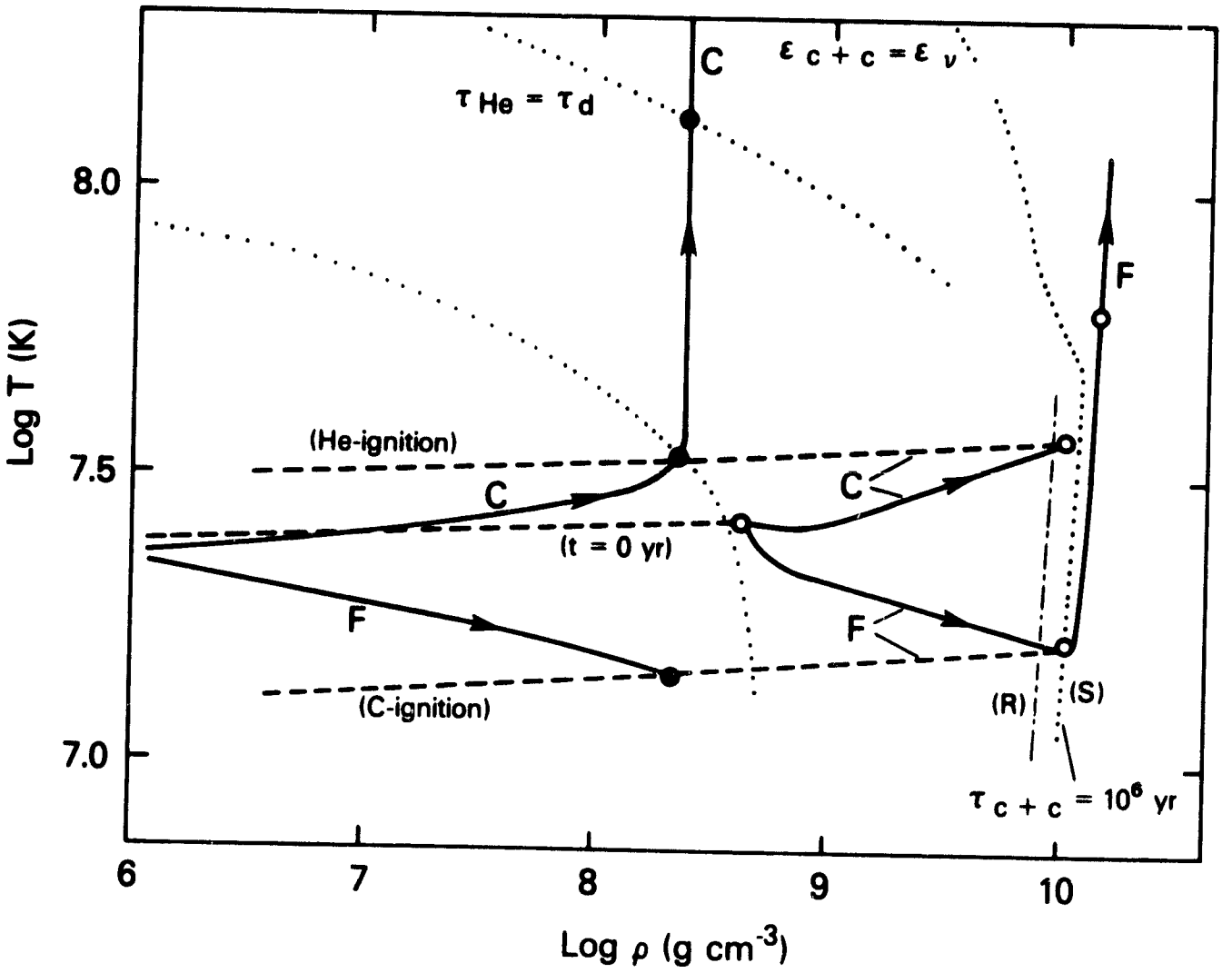
C
$\varepsilon_{c+c} = \varepsilon_{\nu}$
$\tau_{He} = \tau_{d}$
8.0
7.5
7.0
Log T (K)
F
(He-ignition)
C
C
(t = 0 yr)
F
F
(C-ignition)
(R)
(S)
$\tau_{c+c} = 10^{6}$ yr
6
7
8
9
10
Log ρ (g cm^{-3})

Figure 6

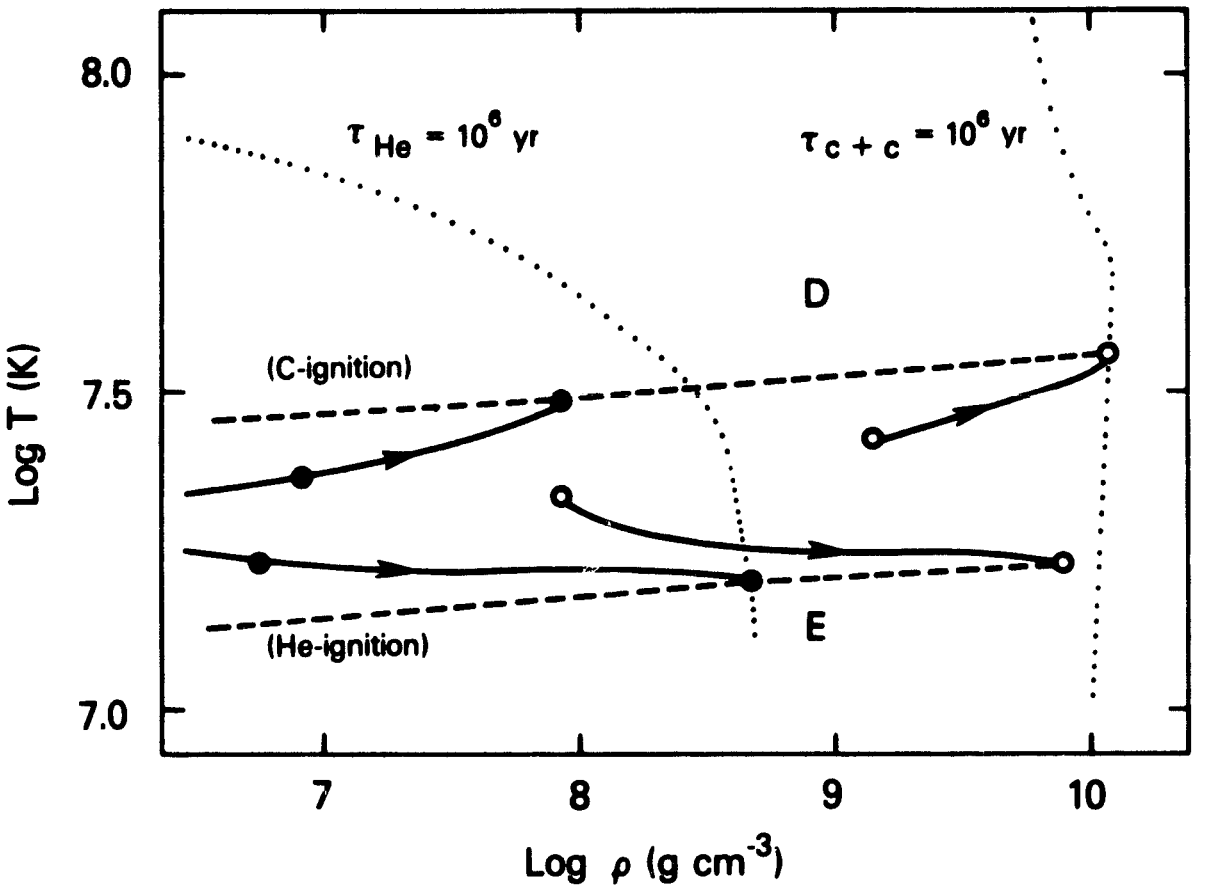
8.0
7.5
7.0
Log T (K)
$\tau_{He} = 10^6$ yr
$\tau_{C+C} = 10^6$ yr
D
(C-ignition)
E
(He-ignition)
7
8
9
10
Log ρ (g cm^{-3})

Figure 7

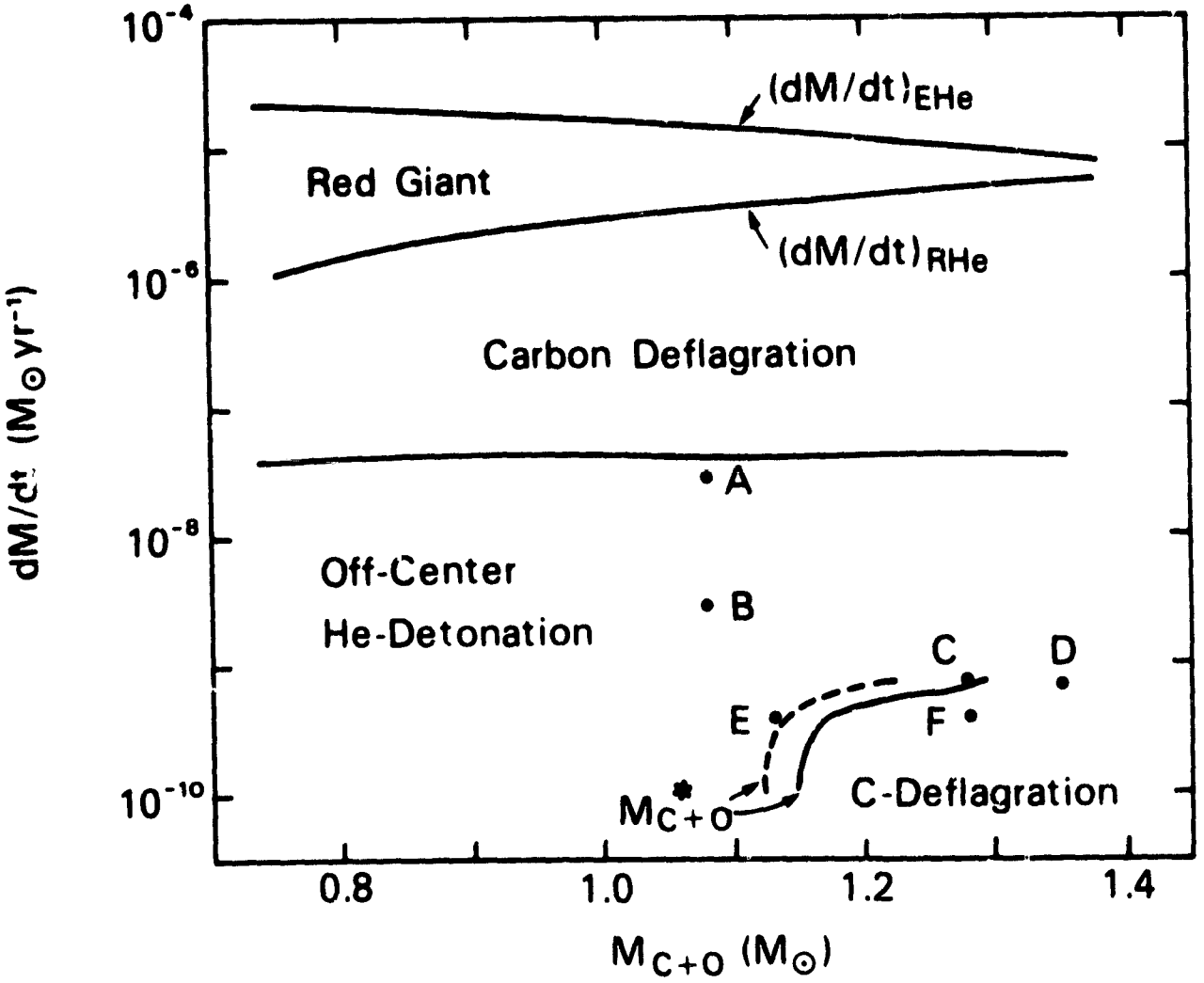
10^{-4}
10^{-6}
10^{-8}
10^{-10}
dM/dt ($M_\odot$ yr^{-1})
$(dM/dt)_{EHe}$
Red Giant
$(dM/dt)_{RHe}$
Carbon Deflagration
A
Off-Center
He-Detonation
B
C
D
E
F
M_{C+O}
C-Deflagration
0.8
1.0
1.2
1.4
M_{C+O} ($M_\odot$)

Figure 8

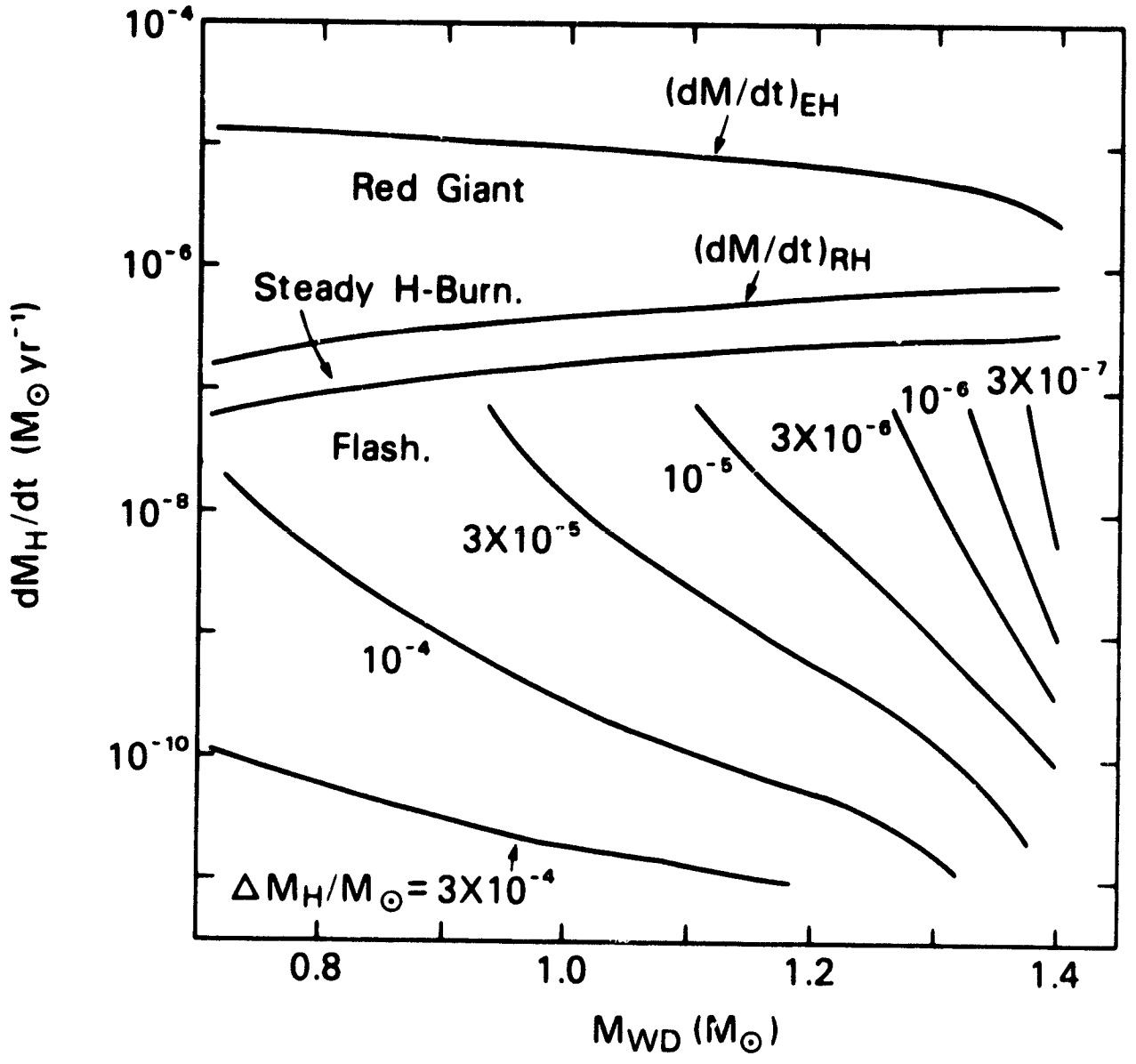
10^{-4}
10^{-6}
10^{-8}
10^{-10}
dM_H/dt ($M_\odot$ yr^{-1})
$(dM/dt)_{EH}$
Red Giant
$(dM/dt)_{RH}$
Steady H-Burn.
Flash.
10^{-5}
$3X10^{-6}$
10^{-6}
$3X10^{-7}$
$3X10^{-5}$
10^{-4}
$\Delta M_H/M_\odot = 3X10^{-4}$
0.8
1.0
1.2
1.4
M_{WD} ($M_\odot$)

Figure 9